International Journal of Fatigue 209 (2026) 109643

Contents lists available at ScienceDirect

International Journal of Fatigue

journal homepage: www.elsevier.com/locate/ijfatigue

Towards understanding the interaction mechanism between the hyperelasticity and fatigue performances of NiTi TPMS lattices by laser powder bed fusion

Yunlong Ren [a], Xiang Liu [b], Lei Yang [a,b,*], Guanghui Yang [a], Liu He [b], Lei Zhou [a], Zhanpeng Pi [b], Hejiang Xu [a], Jinhua Xiao [c], Chunze Yan [b], Yusheng Shi [b]

[a] School of Transportation and Logistics Engineering, Wuhan University of Technology, Wuhan 430063, China
[b] State Key Laboratory of Materials Processing and Die & Mould Technology, School of Materials Science and Engineering, Huazhong University of Science and Technology, Wuhan 430074, China
[c] Department of Management, Economics and Industrial Engineering, Politecnico di Milano, Piazza Leonardo da Vinci 32, 20133 Milan, Italy

ARTICLE INFO

Keywords:
Additive Manufacturing
Triply periodic minimal surface (TPMS)
Hyperelasticity
Fatigue hysteresis

ABSTRACT

The NiTi lattice structure has great application potential in biomedical and aerospace fields, due to the shape memory effect, hyperelasticity and other characteristics. According to the research purpose and material behavior, cyclic compression is divided into hyperelastic cyclic compression and fatigue cyclic compression. Many studies have been conducted, but either to improve the hyperelastic cyclic compression performance or to improve the fatigue cyclic compression performance, no study has yet revealed the connection between the two. Therefore, in this study, hyperelastic cycles (1, 8, 15) were conducted before fatigue cyclic compression, while fatigue cycles (10^4, 5×10^4, 10^5) were conducted before hyperelastic cyclic compression. The results show that the fatigue cyclic compression pretreatment of 10^4 and 5×10^4 cycles helps to improve the hyperelasticity of the lattice structure, while too many fatigue cycles will reduce the hyperelasticity of the structure. Furthermore, the bearing capacity of the sample is enhanced by 10^4 cycles of fatigue cyclic compression pretreatment. On the contrary, the fatigue life of the sample can be increased by 2.49 times after 8 cycles of hyperelastic cyclic compression pretreatment, due to reducing the grain size. This study reveals the interaction mechanism between hyperelasticity and fatigue performances of NiTi lattice structures.

1. Introduction

The NiTi lattice structure has excellent specific strength, good energy absorption performance and damping performance, excellent biocompatibility and impact protection functions[1]. Due to its significant mechanical advantages in low-density structures, it has been often utilized in biological bone implants, shock absorbers[2,3]. As the high-accuracy manufacturing characteristic, laser powder bed fusion (LPBF) is the most commonly used additive manufacturing (AM) technology to fabricate the NiTi lattice structures [4].

However, when the NiTi lattice structures are loaded, their microstructure may undergo irreversible changes, which in turn affect the overall structural performance[5]. Therefore, it is important to understand and optimize the properties of these NiTi lattice structures to ensure the reliability of their work in various environments. There have been many studies on structural design and process treatment, which have improved the mechanical and fatigue properties of NiTi lattice structures[6,7]. Structural design is an important means to improve the mechanical properties of lattice structures. By optimizing the geometry and arrangement of the unit cell, a more uniform stress distribution can be achieved. Gyroid is a kind of Triply Periodic Minimal Surface (TPMS) with complex geometry and uniform pore distribution[8]. Compared with strut-based lattice structures, TPMS lattice structure has a more uniform stress distribution [9] and better fatigue life[10]. The forming quality and mechanical properties of the lattice structure can be significantly improved by process treatment (process parameters and process methods). Zheng et al. [11] explored the effect of nickel plating post-treatment process on the mechanical properties of lattice structures. Hussain et al. [12] studied the effects of additive manufacturing process parameters on the microstructure characteristics and solid phase

* Corresponding author.
E-mail address: yangleihust@hust.edu.cn (L. Yang).

https://doi.org/10.1016/j.ijfatigue.2026.109643
Received 4 December 2025; Received in revised form 12 March 2026; Accepted 18 March 2026
Available online 27 March 2026

distribution in the sample. Liu et al.[13]found that adjusting the process parameters can make NiTi shape memory alloy have high hyperelastic cycle stability. Sun et al. [14] found that the lattice structure prepared by the pressureless infiltration process has higher damping capacity and strength. Kara et al.[15,16] studied the effect of cryogenic treatment on the processing properties of materials. Ren et al. [17]have shown that annealing treatment can enhance the energy absorption capacity of lattice structures. Process treatment technology plays an important role in improving the mechanical properties of lattice structures.

Researchers have conducted many studies on the hyperelasticity and fatigue performances of NiTi lattice structures through cyclic compression experiments. Cyclic compression refers to the process in which a material or structure is subjected to repeated compressive loads over a period of time. According to the research purpose and material behavior, it can be divided into hyperelastic cyclic compression and fatigue cyclic compression[18]. Hyperelastic cyclic compression: The macroscopic reversible deformation characteristics of materials during repeated loading and unloading are studied, focusing on the recoverability and energy absorption efficiency of materials. Kan et al.[19], Safdel et al. [20], Wang et al.[21], Yan et al.[22]and Zhang et al.[23] studied the hyperelasticity of NiTi alloy by hyperelastic cyclic compression test, and summarized the change rule of hyperelasticity and its damage. Fatigue cyclic compression: The phenomenon that the material gradually accumulates damage and eventually leads to failure during repeated loading and unloading is studied, focusing on the fatigue life and damage mechanism of the material [24]. Kelly et al.[25] and Yang et al.[26] studied the fatigue properties of Gyroid by fatigue cyclic compression test, and summarized the change rule and strengthening of fatigue properties.

In the past few decades, many cyclic compression tests have been performed on NiTi alloys[27]. Researchers only focus on the hyperelasticity or fatigue properties of the NiTi lattice structure itself. However, in engineering applications, the NiTi lattice structure may be subjected to both hyperelastic cyclic compression and fatigue cyclic compression. It is not comprehensive to only focus on the hyperelasticity or fatigue properties of the NiTi lattice structure itself. The existing papers have not studied the relationship between hyperelasticity and fatigue performance.

Therefore, the aim of this paper is to systematically investigate the effect of hyperelastic cyclic compression on fatigue performance, as well as, the effect of fatigue cyclic compression on hyperelastic performance.

This study adopts the design idea of hyperelasticity and fatigue interaction. The relationship between mechanical and fatigue properties of NiTi Gyroid lattice structure under cyclic compression was investigated. The structural evolution of NiTi Gyroid lattice structure under cyclic compression and its influence on macroscopic mechanical behavior are revealed.

2. Methodologies

2.1. Design and fabrication

Fig. 1 shows the design idea of the interaction between hyperelastic cyclic compression and fatigue cyclic compression.

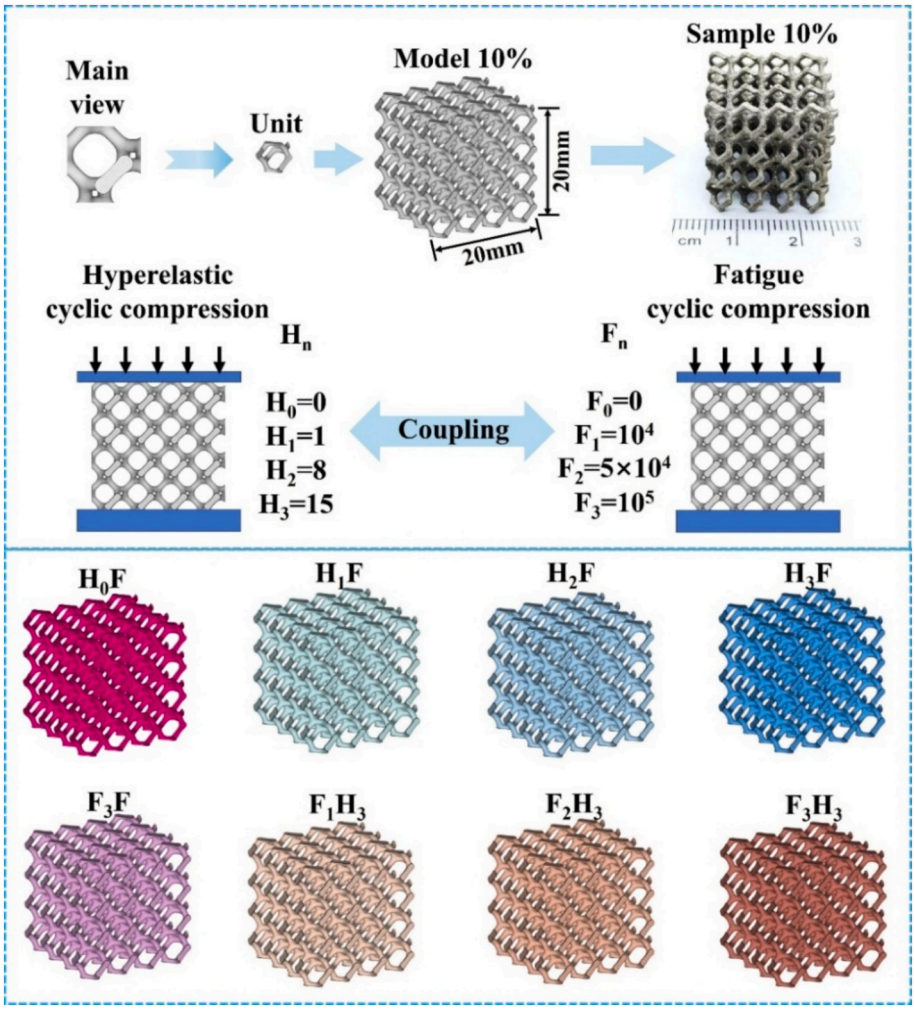

Fig. 1. The design idea of the interaction between hyperelastic cyclic compression and fatigue cyclic compression.

The Gyroid rod structure is selected for research. The Gyroid surface can be expressed by the following equation:

$$sin(\frac{2\pi}{a}\cdot x)cos(\frac{2\pi}{a}\cdot y)+sin(\frac{2\pi}{a}\cdot y)cos(\frac{2\pi}{a}\cdot z)+sin(\frac{2\pi}{a}\cdot z)cos(\frac{2\pi}{a}\cdot x)=t \quad (1)$$

Among them, a refers to the size of the unit cell, and t refers to the volume range surrounded by the minimal surface. As shown in Fig. 1, the volume fraction of both the model and the sample is 10 %. The unit cell size is 5 mm, stacked along the direction of the spatial geometric coordinate system (x, y, z), the model size is 20 mm. The implicit function modeling of TPMS lattice structure can be carried out by inputting the surface equation of Gyroid into Matlab software. This study uses TPMS_Scaffold_Generator software to design, which is a TPMS lattice structure modeling software developed by Lin et al[28].

Samples were prepared by the DiMetal-100 (Laseradd Co., Ltd, China). The particle size of NiTi alloy powder is 15–53 μm, and the atomic ratio of Ni to Ti is 1:1 (Avimetal Powder Metallurgy Technology Co., Ltd., China). After process optimization, the selected process parameters are shown in Table 1. The scanning mode is set to X/Y alternating mode. The whole process needs to be carried out under the protection of argon gas.

As shown in Table.2, different pretreatment and post-processing schemes are applied to the Gyroid rod structure, which can be divided into 8 different schemes: H_0F, H_1F, H_2F, H_3F, F_3F, F_1H_3, F_2H_3, F_3H_3.

The hyperelastic cyclic compression process is recorded as H_n. H_0, H_1, H_2, and H_3 denote the number of hyperelastic cycles of 0,1,8 and 15, respectively. Jin et al. [29] studied the hyperelasticity of NiTi lattice structure. A total of 15 hyperelastic cyclic compression experiments were carried out. The unrecoverable strain curve has a turning point at about the 8th time. As shown in Fig. 3(d)~(i) and Fig. 4(a), the strain of the NiTi lattice structure changes slowly from the 8th cycle under the hyperelastic cyclic compression. Therefore, the number of hyperelastic cycles of 0,1,8 and 15 were selected for this study.

The fatigue cyclic compression process is recorded as F_n. F_0, F_1, F_2, and F_3 represent the number of fatigue cycles of 0, 10^4, 5×10^4 and 10^5, respectively. The study of Liu et al.[30] showed that the NiTi lattice structure with a volume fraction of 10 % will break under certain conditions after 2×10^5 cycles of fatigue cyclic compression. In this paper, 5 %, 10 % and 50 % of the fatigue life (2×10^5) are selected as the fatigue pretreatment cycle conditions (10^4, 5×10^4 and 10^5). As shown in Fig. 5(b), when the fatigue loading stress is 3.23 Mpa, the fatigue life of the NiTi lattice structure is 190,020 cycles. In order to save the time consumed by the fatigue test, this study selected a fatigue loading stress value of 3.23 Mpa for fatigue cyclic compression pretreatment.

2.2. Measurement and characterization

The size of samples was measured using a vernier caliper (minimum scale increment of 0.01 mm). The weight of samples was measured using an electronic balance (minimum scale increment of 0.1 mg). The relative density and actual volume fraction of the lattices can be calculated by characterizing the size and mass. The design volume fraction (V_{design}) is 10 %, and the actual volume fraction (V_{actual}) can be obtained by Archimedes' principle[31]. The actual density ρ_a and relative density RD (Relative density) of the sample entity can be obtained by the following formula [31]:

$$\rho_a=\frac{m_1}{m_1-m_2}\rho_0 \quad (2)$$

$$RD=\frac{\rho_a}{\rho_{power}}\times100 \quad (3)$$

Among them, m_1 is the dry weight of the sample, m_2 is the floating weight of the sample, and ρ_0 is the density of the liquid. In this study, ρ_0 represents industrial alcohol with a density of 0.81 g/cm^3, and ρ_{power} is the density of NiTi alloy powder, which is 6.45 g/cm^3.

Scanning electron microscopy (SEM) was used to observe the microstructure of the samples (Field emission scanning electron microscope JSM-7600F, Japan). SEM is very powerful in providing high-resolution topography images. The NiTi samples can be directly put into the loading table for testing after being cleaned by vacuum cleaner.

The electron backscattered diffraction (EBSD) technique was used to characterize the internal grain distribution of the sample (Zeiss Sigma 300, Oxford spectrum ULTIM MAX 40, Oxford EBSD C-SWIFT, British), and the experimental step was 1. Firstly, the samples were cut into small samples of 8 mm × 8 mm × 5 mm by wire electrical discharge machining. Then the surface of the sample was treated by argon ion polishing technology. Finally, the samples were put into the equipment for experiments.

2.3. Mechanics and fatigue performance test

The mechanical properties of the structure under uniaxial compression were tested by material performance testing machine (AG-IC 100 kN, Japan). According to ISO 13314: 2011 [32], metal materials are subjected to compression tests at a strain rate of 0.1 %S^{-1}. All samples are placed in the same way and the compressive loading speed was set to be 1.2 mm / min. Two samples were tested in each group.

The hyperelastic cyclic compression test was carried out by material performance testing machine (AG-IC 100 kN, Japan). The test needs to set the cyclic compression displacement, compression speed and the number of cycles. The cyclic compression displacement is 8 % of the designed size of the sample, the compression speed is 1.2 mm / min, and the number of cycles is 1,8 and 15, respectively. The upper compression platform moves back and forth to achieve the set number of cycles.

The fatigue test was carried out by hydraulic test frame (EHF-UV100k2-040-1A, Japan). The loading frequency is 30 Hz, and the load ratio R is 0.1. In this experiment, 10^6 cycles were selected as the end cycle of the experiment. Set the lower limit position to control that the machine will stop immediately after the sample fails. In this study, a S-N diagram of NiTi Gyroid sample with a volume fraction of 10 % treated by H_0F was constructed. The corresponding fatigue loading stress points are shown in Table.3. σ_y refers to the strength limit when the external force is pressure. In this study, the fatigue loading condition selected by F_n is the loading stress value of 0.35σ_y (3.23 MPa).

2.4. Finite element analysis

The ideal lattice structure model was meshed by HyperMesh (2019 version) and divided into 70,590 C3D10M units. C3D10M is an improved version of the quadratic tetrahedron element, which can accurately describe complex surfaces (such as the curved surface of the TPMS structure)[33]. The use of C3D10M element can significantly improve the simulation accuracy and convergence of complex structures such as TPMS in large deformation and contact analysis[29]. The meshed model is imported into ABAQUS (2020 version), and the explicit dynamic analysis is adopted[29].

Table 1
LPBF process parameter.

Layer thickness (mm)	Scanning strategy	Energy density (J/mm^3)	Laser power (W)	Scanning speed (mm/s)
0.04	Post-output	56.1	220	1400

Table 2
Naming rules of samples.

processing steps		H_0F	H_1F	H_2F	H_3F	F_3F	F_1H_3	F_2H_3	F_3H_3
Pretreatment cycle	Hyperelastic cyclic	0	1	8	15	0	0	0	0
	Fatigue cyclic	0	0	0	0	10^5	10^4	5×10^4	10^5
post-processing	Hyperelastic cyclic 15 times	no	no	no	no	no	yes	yes	yes
	Fatigue cyclic	yes	yes	yes	yes	yes	no	no	no

Table 3
Fatigue loading stress selection of NiTi Gyroid sample.

Sample	$0.3\sigma_y$ (MPa)	$0.35\sigma_y$ (MPa)	$0.4\sigma_y$ (MPa)	$0.45\sigma_y$ (MPa)
NiTi Gyroid	2.76	3.23	3.69	4.15

3. Results and discussion

3.1. Forming quality

The relative density of the sample is shown in Fig. 2(a). Six groups of samples were selected. The minimum relative density was 99.28 %, indicating that the samples studied in this paper had good forming quality[34].

The volume fraction can reflect the manufacturing fidelity[35]. As shown in Fig. 2 (b), six groups of samples were selected, and the actual volume fraction of each group of samples was above 10 %. The actual volume fraction of the sample is higher than the design volume fraction of the model, which is mainly due to the expansion of the molten pool and the adhesion of the powder particles[36]. Yang et al.[37]showed that the degree of powder adhesion was positively correlated with the specific surface area (the ratio of surface area to volume) of the lattice structure.

Fig. 2(c1)~(c4) shows the SEM images of NiTi Gyroid sample nodes and pillars. The surface of the sample is rough, while the contour is complete without obvious defects. The samples characterized by SEM experiments are before loading. As shown in Fig. 2(c1) and (c2), yellow line segments illustrate that some stripes can be observed on the upper surface of the lattice structure pillars and nodes in the main view, that is, the step effect of the additive manufacturing process[38]. As shown in Fig. 2(c3) and (c4), the lower surfaces of the joints and struts are rougher and the phenomenon of powder adhesion is rather serious.

3.2. Effect of fatigue cycles on hyperelasticity and bearing capacity

3.2.1. Uniaxial compression and hyperelastic cyclic compression

As shown in Fig. 3(a), the mechanical response of NiTi Gyroid sample during compression is divided into three stages[39]: elastic deformation stage, elastic–plastic deformation stage and stress fluctuation stage. The stress–strain images of the same samples prepared in this study are consistent, which indicates that the samples prepared by LPBF have good repeatability.

The static simulation analysis of NiTi Gyroid structure is shown in Fig. 3(b). The red area of the stress cloud diagram indicates that the structure has a large stress concentration here. The results of the stress cloud diagram show that there is a greater stress concentration in the middle of the pillar when subjected to compressive load. This result is also consistent with the fracture situation in Fig. 3(c). The NiTi Gyroid

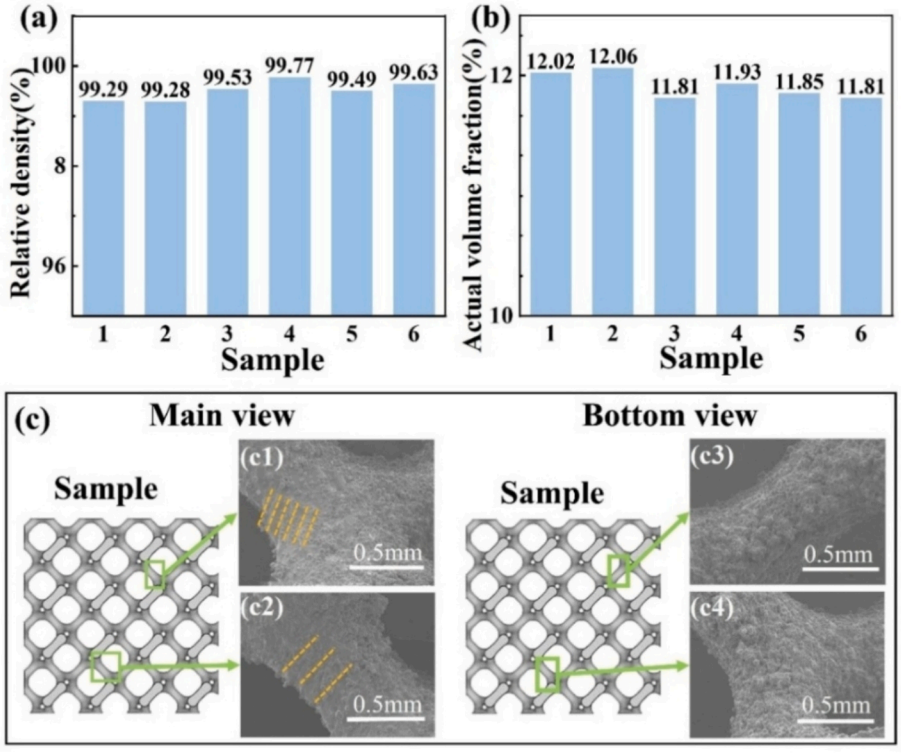

Fig. 2. Forming accuracy and surface morphology of NiTi Gyroid samples: (a) relative density; (b) volume fraction; (c) surface morphology.

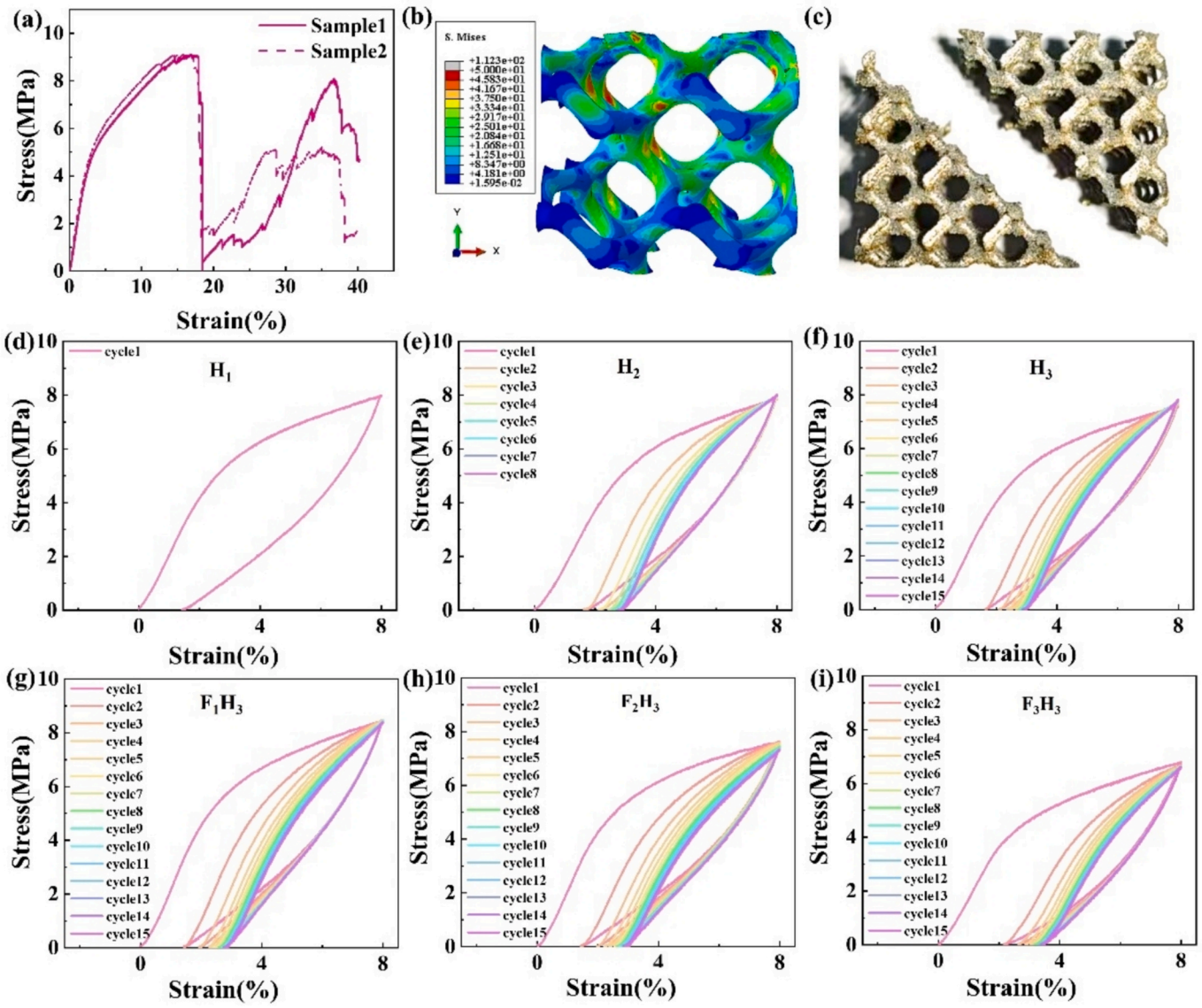

Fig. 3. Uniaxial compression performance and hyperelastic cyclic compression performance: (a) stress–strain curve of uniaxial compression; (b) stress cloud; (c) fracture diagram; (d) H_1 ; (e) H_2 ; (f) H_3 ; (g) F_1H_3 ; (h) F_2H_3 ; (i) F_3H_3.

sample fractured along the middle of the pillar, forming a 45° fracture zone.

H_1, H_2 and H_3 indicate that the samples are subjected to 1,8 and 15 cycles of hyperelastic cyclic compression, respectively. Fig. 3(d)~(f) represent the cyclic compressive stress–strain curves corresponding to the hyperelastic cyclic compression process of H_1, H_2 and H_3, respectively. The cyclic compressive stress–strain curve of Fig. 3(d) is consistent with the first cycle of Fig. 3(e). The cyclic compressive stress–strain curve of Fig. 3(e) is consistent with the first 8 cycles of Fig. 3(f). This shows that the mechanical properties of the same samples manufactured by additive manufacturing are similar.

F_1H_3, F_2H_3 and F_3H_3 represent that the samples undergo fatigue cyclic compression of 10^4, 5×10^4 and 10^5cycles, respectively, and then undergo hyperelastic cyclic compression of 15 cycles. Fig. 3(g)~(i) show the cyclic compressive stress–strain curve corresponding to 15 cycles of hyperelastic cyclic compression processes of F_1H_3, F_2H_3 and F_3H_3 samples. The stress–strain curve of the sample shifts to the right with the increase of the number of cyclic compression cycles. However, after the 8th cycle of cyclic compression, the subsequent cyclic compression stress–strain curve of the sample almost does not change. In this study, 1,8 and 15 cycles were selected as the number of hyperelastic cyclic compressions mainly for this reason. The results of Fig. 3(g)~(i) show that with the increase of the number of pretreatment fatigue cycles, the bearing capacity of the structure decreases.

3.2.2. *Further discussion on hyperelastic enhancement*

As shown in Fig. 4(a), with the increase of hyperelastic cycles, H_2 and H_3 have the same change trend. It is obvious that the strain of F_1H_3 in each cycle is less than that of H_3, indicating that the fatigue cycle has positive effect on the hyperelastic performance. However, the unrecovered strain of each cycle of F_3H_3 is much higher than that of H_3. This may be due to the fact that the internal structure of the sample is more prone to large deformation after 10^5 cycles of fatigue cyclic compression pretreatment.

As shown in Fig. 4(b), H2 and H3 have the same change trend with the increase of the number of cycles. It is worth noting that the stress change values of H_2 and H_3 are between 7.5 MPa and 8.0 MPa. The stress of F_1H_3 in each cycle is greater than that of the other four samples, which may be due to the fact that the fatigue cyclic compression of 10^4 cycles hardens the microstructure inside the sample. However, with the increase of the number of cycles, the stress of F_1H_3, F_2H_3 and F_3H_3 gradually decreases. The stress values of F_2H_3 and F_3H_3 are less than that of

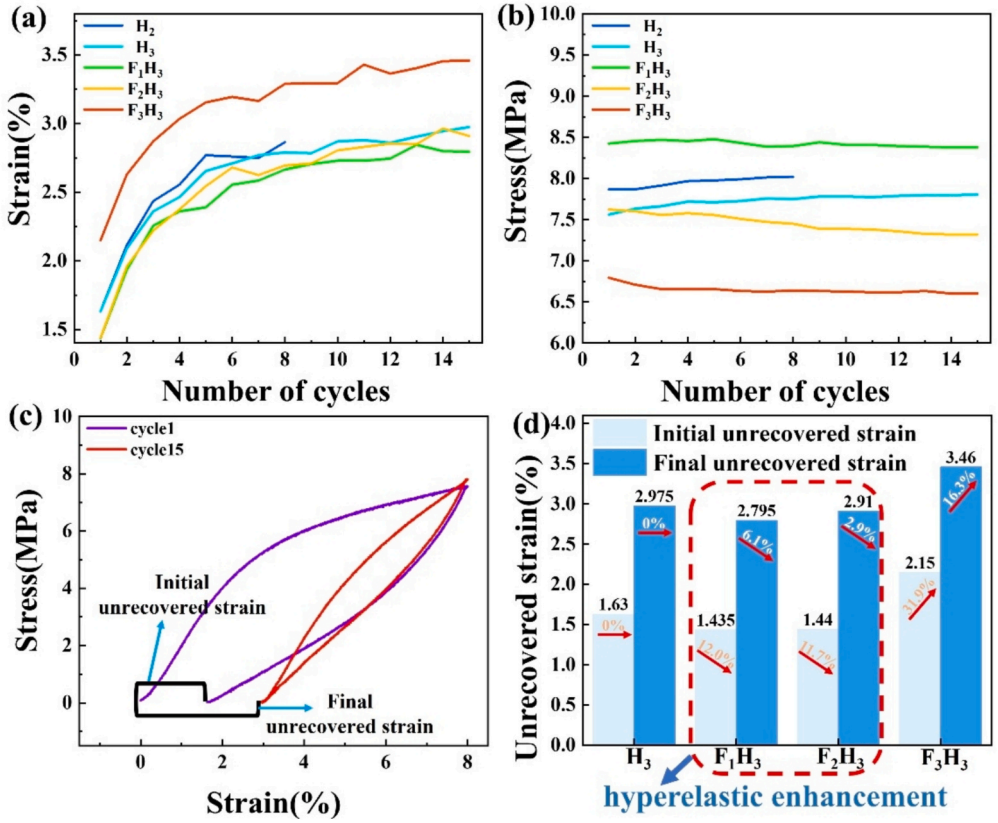

Fig. 4. Hyperelastic analysis: (a) the change of unrecovered strain with the number of cycles; (b) the stress corresponding to the strain of 8 % changes with the number of cycles; (c) unrecovered strain; (d) unrecovered strain contrast diagram.

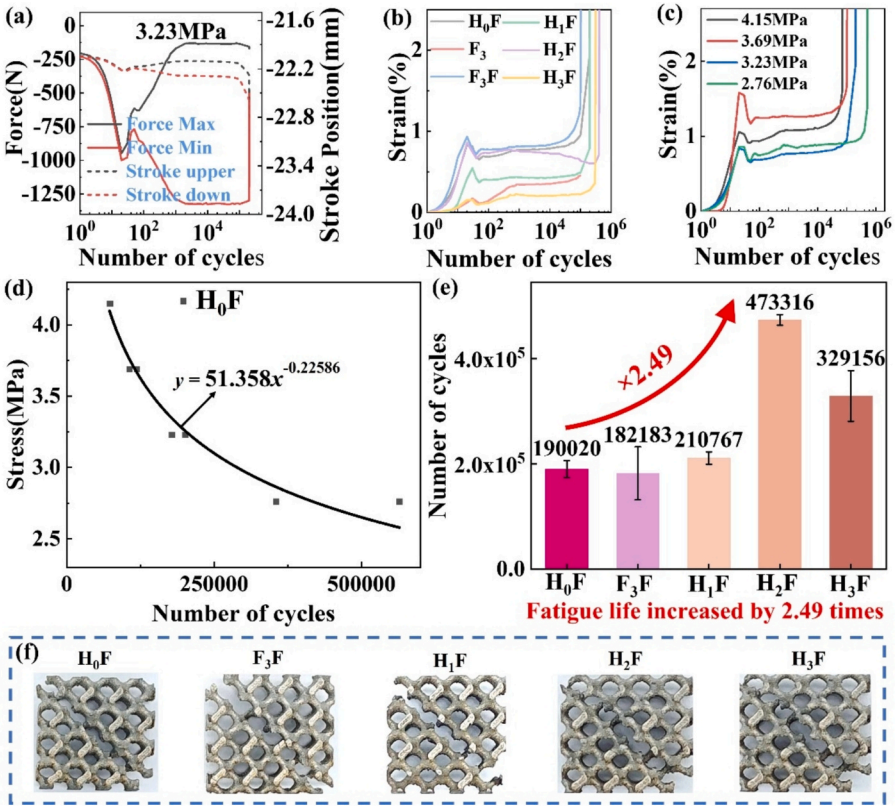

Fig. 5. Strain accumulation and fatigue life: (a) test platform; (b) cumulative strain of different samples; (c) cumulative strain of H_0F under different stress conditions; (d) S-N diagram of H_0F(N refers to the number of cycles in this study); (e) fatigue life improvement diagram; (f) fatigue fracture of the samples.

H_3. This indicates that the fatigue cycle compression of 10^5 and 5×10^4 cycles cause the internal structure of the sample to be destroyed.

To further investigate the change of the hyperelasticity, the unrecovered strain of the NiTi lattice structure is studied. Fig. 4(c) shows the first-cycle cyclic compression and the fifteenth-cycle cyclic compression of C_3. For H_3, the first cycle is the initial cyclic compression cycle, and the 15th cycle is the final cyclic compression cycle. The unrecoverable strain of the initial cyclic compression cycle is defined as the initial unrecoverable strain, and the unrecoverable strain of the final cyclic compression cycle is defined as the final unrecoverable strain[40].

Fatigue cyclic compression pretreatment can enhance the hyperelasticity of NiTi lattice structure. Fig. 4(d) shows the unrecovered strain comparison of F_1H_3, F_2H_3, H_3 and F_3H_3 samples. As shown in the orange and white numbers, F_1H_3 is compared to H_3. The initial unrecovered strain decreased by 12.0 %, and the final unrecovered strain decreased by 6.1 %. F_3H_3 is compared to H_3. The initial unrecovered strain increased by 31.9 %, and the final unrecovered strain increased by 16.3 %. The initial unrecovered strain and the final unrecovered strain of F_1H_3 and F_2H_3 are smaller than H_3, which indicates that the fatigue cyclic compression of 10^4 and 5×10^4 cycles can improve the hyperelasticity of NiTi Gyroid samples.

3.3. Effect of hyperelastic cycles on fatigue properties

3.3.1. Fatigue performance enhancement

At the beginning of the test, the operation of the fatigue equipment was unstable. As shown in Fig. 5(a), the equipment operation under the loading condition of 3.23 MPa ($0.35\sigma_y$) is shown. At the beginning of the test, the force applied by the device to the sample will suddenly increase, and then change rapidly and stabilize to the set load value. The fatigue test equipment reaches stability in the 3000th cycle.

H_0F indicates that the sample is directly subjected to fatigue cyclic compression. F_3 indicates that the sample only undergoes 10^5 cycles of fatigue cyclic compression, while, F_3F indicates that the sample was suspended during 10^5 cycles of fatigue cyclic compression, and then subjected to fatigue cyclic compression. H_1F, H_2F and H_3F indicate that the samples are subjected to 1,8 and 15 cycles of hyperelastic cyclic compression, respectively, and then subjected to fatigue cyclic compression. Fig. 5(b) shows the cumulative strain-period curves corresponding to six different fatigue processes. The comparison of the cumulative strain curves of F_3 and F_3F shows that the cumulative strain of the structure will be significantly increased by suspending the experiment after 10^5 cycles of fatigue without replacing the sample and restarting the fatigue experiment. The comparison of the cumulative strain curves of H_1F, H_2F and H_3F shows that the fatigue cumulative strain of the sample with 1 cycle of hyperelastic cyclic compression is small during fatigue. Moreover, the sample has the smallest cumulative strain after 15 cycles of hyperelastic cyclic compression. The fatigue cumulative strain of the sample after 8 cycles of hyperelastic cyclic compression is large. Hyperelastic cyclic compression pretreatment is beneficial to enhance the deformation resistance of the NiTi lattice structure.

Fig. 5(c) shows the cumulative strain-period curves of H_0F under different stress conditions. With the increase of load value, the cumulative strain of H_0F shows a trend of increasing. However, the cumulative strain of H_0F under the load condition of 3.69 MPa ($0.4\sigma_y$) is higher than that of 4.15 MPa ($0.45\sigma_y$). This is closely related to the "functional fatigue" mechanism of materials under high stress[41,42].

The S-N curve of NiTi Gyroid sample with volume fraction of 10 % after H_0F treatment is shown in Fig. 5(d). The higher the stress level, the lower the fatigue life of the NiTi Gyroid sample. In this study, 3.23 MPa ($0.35\sigma y$) was selected as the fatigue loading condition, and the fatigue life comparison diagram of NiTi Gyroid samples corresponding to five different cyclic compression pretreatments at 3.23 MPa ($0.35\sigma y$) was constructed, as shown in Fig. 5(e). In Fig. 5(f), the fatigue fracture directions of the samples are all along 45°.

The fatigue life of F_3F is close to H_0F, which indicates that the fatigue life of the sample is less affected by the suspension of fatigue after 10^5 cycles. However, the error bar of fatigue life is larger. The fatigue life of H_3F is much lower than that of H_2F, which may be due to the destruction of the internal structure of NiTi Gyroid sample after 15 cycles of compression. In Fig. 4(a), it is noted that the unrecovered strain of the NiTi Gyroid sample does not change after 8 cycles of hyperelastic cyclic compression. This shows that after 8 cycles of hyperelastic cyclic compression, the internal structure of the NiTi Gyroid sample may be destroyed, which in turn causes a change in fatigue life. The fatigue life of H_1F is slightly improved compared with that of H_0F. It is worth noting that the fatigue life of H_2F and H_3F is greatly improved compared with H_0F. The fatigue life of H_2F is 2.49 times that of H_0F. The fatigue life of H_3F is 1.73 times that of H_0F. This shows that the hyperelastic cyclic compression greatly improves the fatigue life of NiTi Gyroid samples.

3.3.2. Hysteresis curve and fatigue damage

The hysteresis curves of six different fatigue processes were obtained from the fatigue test data under the stress level of 3.23 MPa ($0.35\sigma y$). As shown in Fig. 5(a), the change of load and indenter position of fatigue test equipment is not stable at the beginning, and it is stable in the 3000th cycle. In order to obtain more accurate results, the hysteresis curve analysis of NiTi Gyroid sample starts from the 5000th cycle. Fig. 6 (a) ~ (c) show the hysteresis curves of H_0F, F_3 and F_3F. The hysteresis curves shift to the right with the increase of period, showing obvious cyclic ratchet effect. It is worth noting that the span of the hysteresis loop is getting larger and larger in the final stage of the hysteresis curve of F_3F. Fig. 6 (d) ~ (f) show the hysteresis curves of H_1F, H_2F and H_3F. The hysteresis curves of H_1F and H_3F move right along the strain axis. However, when $5000 \leq N \leq 200000$, the hysteresis curve of H_2F shifts to the left along the strain axis. When $200000 \leq N \leq 400000$, the hysteresis curve of H_2F shifts to the right along the strain axis.

The strain region of H_2F hysteresis curve is significantly smaller than that of H_0F, H_1F and H_3F. With the increase of the cycle period, the hysteresis curves of H_0F and H_1F change more violently. H_2F has a strong ability to resist deformation. H_0F, F_3, F_3F, H_1F and H_3F have fatigue crack initiation and propagation during fatigue[43].

The cyclic ratcheting strain and fatigue damage strain of six different fatigue processes were calculated from the hysteresis curve, as shown in Fig. 6(g)~(l). In this study, the cyclic ratcheting strain curve and fatigue damage strain curve of NiTi lattice structure are based on the 5000th cycle. The cyclic ratcheting strain is defined as the offset of the minimum strain of the hysteresis curve of each cycle relative to the minimum strain of the reference cycle (the 5000th cycle), which can represent the material damage caused by the accumulation of plastic deformation. The fatigue damage strain is defined as the variation of the maximum and minimum strain difference of the current cycle relative to the base cycle (5000th cycle), which can represent the material damage caused by the accumulation of fatigue damage[44].

The cyclic ratcheting strains of H_0F, F_3 and F_3F are higher than the fatigue damage strains. This shows that the cyclic ratcheting strain plays a leading role in the fatigue failure of these three structures. The cyclic ratcheting strains of H_1F and H_3F are higher than the fatigue damage strains at lower cycles. This shows that the cyclic ratcheting strain plays a leading role in the failure of the two structures at lower cycle times. For H_2F, the cyclic ratcheting strain is lower than the fatigue damage strain. This shows that the fatigue damage strain plays a leading role in H_2F fatigue failure. Hyperelastic cyclic compression changes the fatigue failure mode of NiTi lattice structure.

It can be seen from Fig. 5(e) that the fatigue life of H_2 is 473,316 cycles, and the fatigue life of H_0 is 190,020 cycles. The fatigue life of the NiTi lattice sample after 8 cycles of hyperelastic cyclic compression is 2.49 times that of the sample without any pretreatment. The fatigue performance of the NiTi lattice can be improved by hyperelastic cyclic compression pretreatments with appropriate cycles.

In order to explore the effect of hyperelastic cyclic compression and

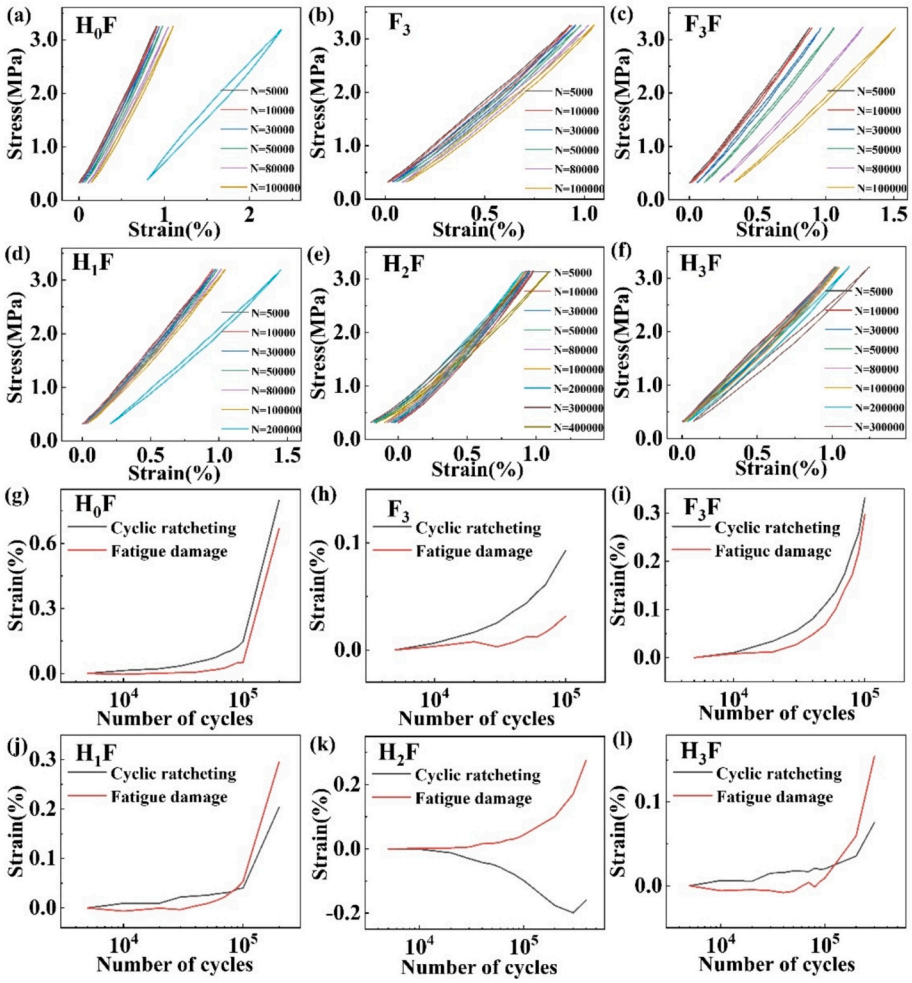

Fig. 6. Hysteresis curve: (a) H_0F ; (b) F_3 ; (c) F_3F ; (d) H_1F ; (e) H_2F ; (f) H_3F. Cyclic ratcheting strain and fatigue damage strain: (g) H_0F ; (h) F_3 ; (i) F_3F ; (j) H_1F ; (k) H_2F ; (l) H_3F.

fatigue cyclic compression on the internal structure of NiTi Gyroid samples, EBSD test was carried out in this study, and the grain distribution of the samples was obtained. Fig. 7 shows the microstructure of NiTi Gyroid structure under hyperelastic cyclic compression and fatigue cyclic compression. Among them, the EBSD test analyzes planes inside the sample. The planes are parallel to the additive manufacturing forming plane. The planes are perpendicular to the direction of cyclic compression loading.

Fig. 7(a1)~(d1) show the secondary electron diagrams (secondary electron, SE) of the samples after argon ion polishing. The volume change caused by the liquid–solid transition during the solidification process did not supplement in time, resulting in micropores [45].

Inverse Pole Figure (IPF) is a commonly used crystal orientation visualization tool in electron backscatter diffraction technology, which is used to display the relationship between the orientation distribution of grains in the sample and a specific reference direction[46]. As shown in Fig. 7, IPF-1 is the crystal orientation distribution image of all electronic image shooting areas, and IPF-2 is the crystal orientation distribution image of small electronic image shooting areas. There are coarse grains and fine grains in the microstructure of LPBF NiTi lattice [47]. A large number of fine grains appear on the boundary of coarse grains. The results of (a3) ~(d3) in Fig. 7 show that the long coarse grains become finer after the hyperelastic cyclic compression pretreatment.

3.3.3. *Further discussion on fatigue performance improvement*

As shown in Fig. 8, the grain size distributions of IPF-1 region and IPF-2 region were calculated. The change and distribution of grain size under hyperelastic cyclic compression and fatigue cyclic compression are shown. D50 represents the grain size when the area-weighted fraction cumulation percentage is 50 %. As shown in Table.4, the area weighted average of the grain size in the IPF-1 region is calculated.

Compared (a1) and (b1) in Fig. 8, the D50 values of H_0 and H_2 are consistent. However, there are obvious differences in the distribution of grain size, and the distribution range of grain size of H_2 is small. Compared (a2) and (b2) in Fig. 8, the D50 value of H_2 is larger and the distribution range of grain size is smaller. The data in Table.4 show that the area weighted average of the grain size of H_2 becomes smaller. This shows that after 8 cycles of hyperelastic cyclic compression pretreatment, the area weighted average of the grain size of the sample decreases, and the grain size distribution range becomes smaller.

Compared (a1) and (c1) in Fig. 8, the D50 value of H_0F is larger, the distribution range of grain size is larger, and there are more large-sized grains. Compared (a2) and (c2) in Fig. 8, the D50 value of H_0F is larger and the distribution range of grain size is larger. The data in Table.4 show that the area weighted average of the grain size of H_0F becomes larger. This shows that after the fatigue cyclic compression treatment, the area weighted average of the grain size of the sample increases, and the grain size distribution range becomes larger.

Compared (b1) and (d1) in Fig. 8, the D50 value of H_2F is smaller and the distribution range of grain size is smaller. Compared (b2) and (d2) in Fig. 8, the D50 value of H_2F is smaller and the distribution range of grain size is smaller. The data in Table.4 show that the area weighted average

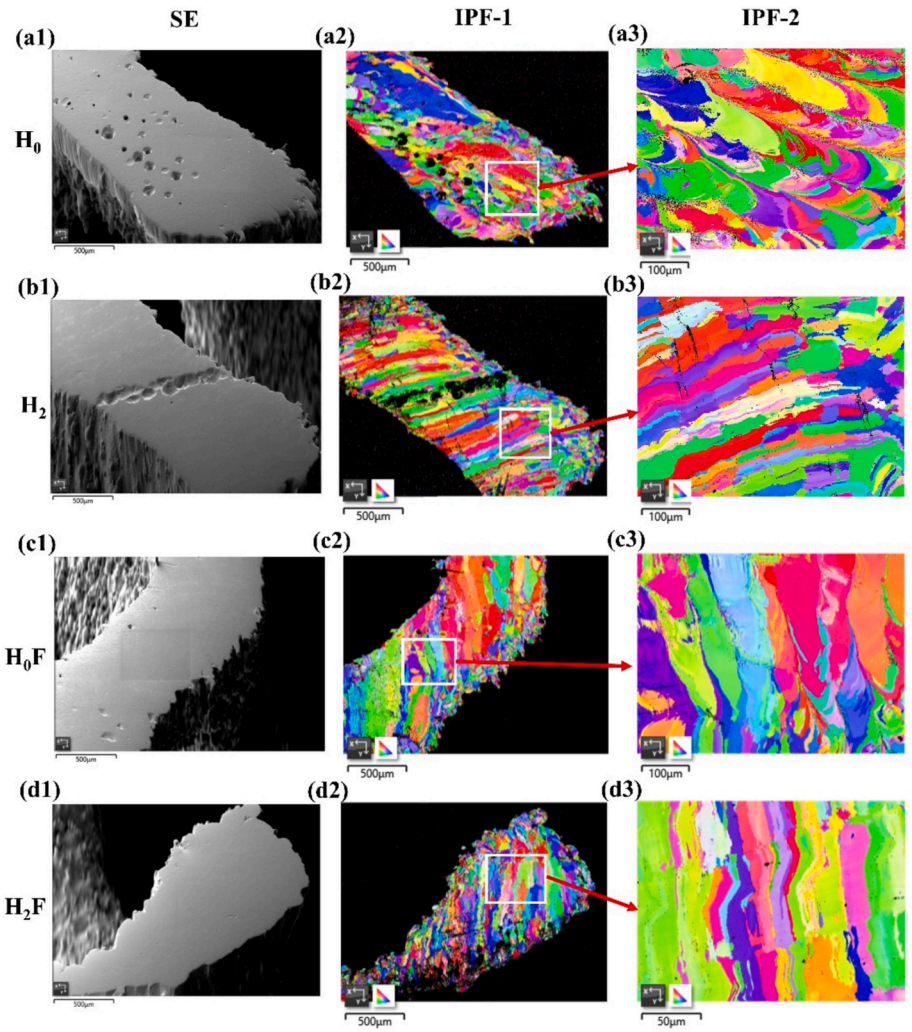

Fig. 7. Microstructure of NiTi Gyroid structure: (a1)~(a3) H_0 ; (b1)~(b3) H_2 ; (c1)~(c3) H_0F ; (d1)~(d3) H_2F.

of the grain size of H_2F becomes smaller. This shows that after 8 cycles of hyperelastic cyclic compression pretreatment and fatigue cyclic compression treatment, the area weighted average of the grain size of the sample decreases, and the grain size distribution range becomes smaller. Compared with the results of H_0F, it is found that the hyperelastic cyclic compression will further affect the change of the grain size of the sample during fatigue and narrow the range of grain size distribution.

Hyperelastic cyclic compression improves the fatigue life of NiTi lattice structure by reducing the area weighted average of the grain size and reducing its size distribution range. This shows that the fatigue performance of LPBF NiTi lattice structure can be further affected by reducing the grain size.

3.4. Interaction of hyperelasticity and fatigue performances

3.4.1. Introduction of the interaction

Fig. 9 shows the interaction between hyperelastic cyclic compression and fatigue cyclic compression. Fig. 7 shows that there are coarse grains and fine grains in the NiTi lattice structure of additive manufacturing, and fine grains are distributed on the boundary of coarse grains. Fig. 8 shows that the grains of NiTi lattice structure change after cyclic compression.

The changes in the internal structure of the NiTi lattice structure after hyperelastic cyclic compression are shown in Fig. 9(a). It is mainly reflected in that the long coarse grains become finer, the area weighted average of grain size becomes smaller, and the distribution range of grain size becomes smaller.

The changes in the internal structure of the NiTi lattice structure after fatigue cyclic compression are shown in Fig. 9(b). It is mainly reflected in that the long coarse grains become coarser, the area weighted average of grain size becomes larger, and the distribution range of grain size becomes larger.

This study summarizes the interaction between hyperelastic cyclic compression and fatigue cyclic compression. As shown in Fig. 9(c), the NiTi lattice structure after hyperelastic cyclic compression was subjected to fatigue test, and the fatigue performance was significantly improved. It is worth noting that the hyperelastic cyclic compression has a higher priority, the hyperelastic cyclic compressed NiTi lattice structure after fatigue, the area weighted average of grain size of the sample decreases, and the grain size distribution range becomes smaller. After a certain number of cycles of fatigue cyclic compression, the hyperelastic test of NiTi lattice structure was carried out, and the hyperelastic energy was significantly improved, and its bearing capacity was enhanced.

3.4.2. Further discussion on the interaction

Song et al.[48] proposed that grain refinement can enhance the resistance to fatigue crack initiation and propagation through grain boundary strengthening and dislocation strengthening. The experimental results of Fintová et al.[49] show that materials with fine-grained or ultrafine-grained structures exhibit better fatigue life than coarse-grained materials. The fundamental reason is the enhancement of

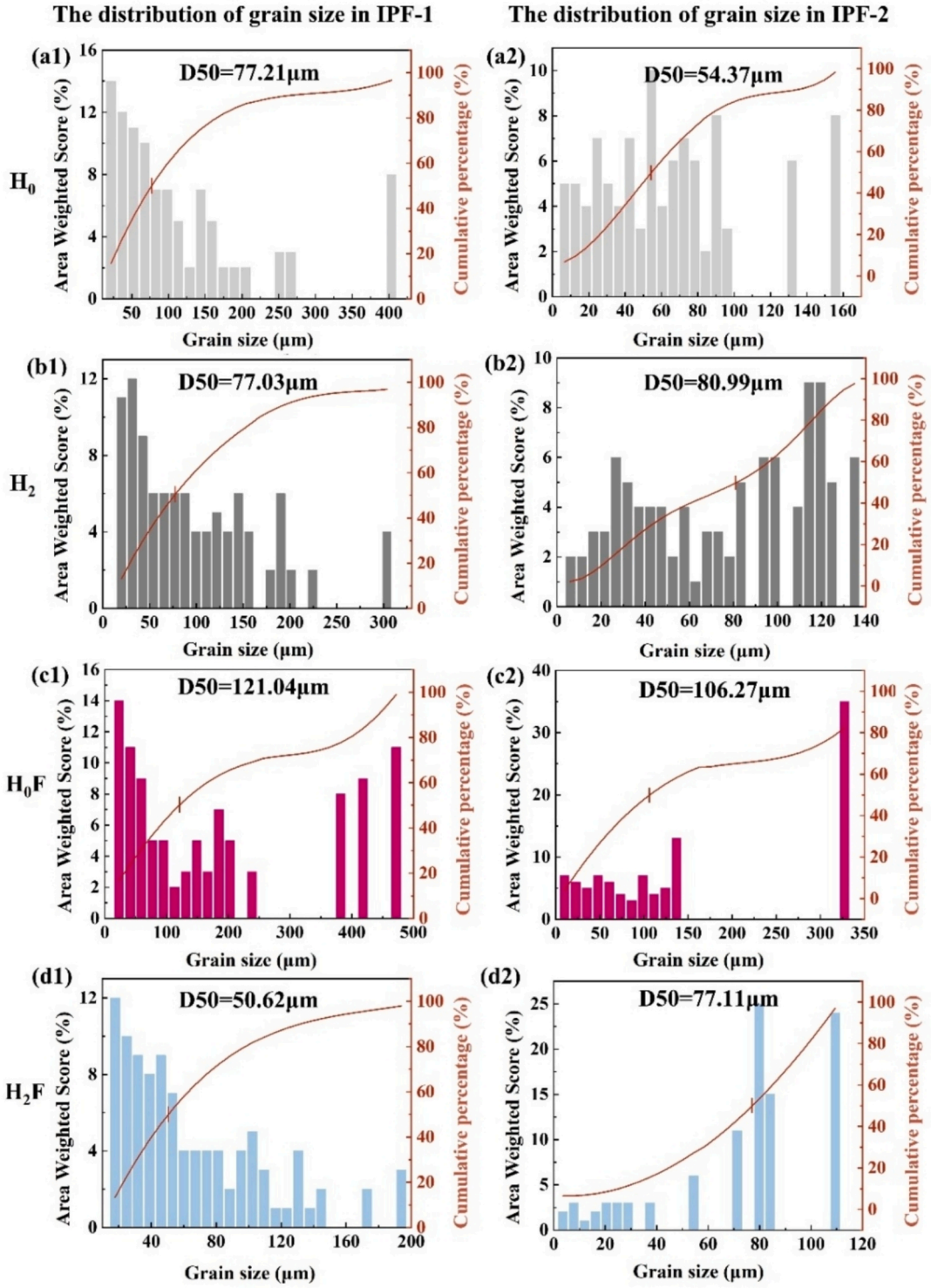

Fig. 8. Grain size statistics: (a1) ~ (d1) statistical results of grain size in IPF-1 region; (a2) ~ (d2) statistical results of grain size in IPF-2 region.

Table 4
The area weighted average of the grain size in the IPF-1 region.

NiTi Gyroid sample	H_0	H_2	H_0F	H_2F
Area weighted average of grain size/(μm)	118.34	98.68	191.97	66.51

grain boundary strengthening effect and the significant delay of crack initiation process. The beneficial effect of grain refinement on fatigue properties is highly consistent with the expected physical mechanism under cyclic hyperelastic deformation conditions.

In hyperelastic alloys, highly reversible stress-induced phase transitions promote the formation of subgrain structures and low-angle grain boundaries. These substructures can be used as effective nucleation sites for further grain refinement in subsequent cyclic loading, and their evolution behavior is similar to the dynamic recovery and dynamic recrystallization processes reported in cyclic deformation studies[50]. The H_2F sample subjected to pre-hyperelastic cyclic refinement exhibits further local grain refinement after fatigue, which is due to the fact that

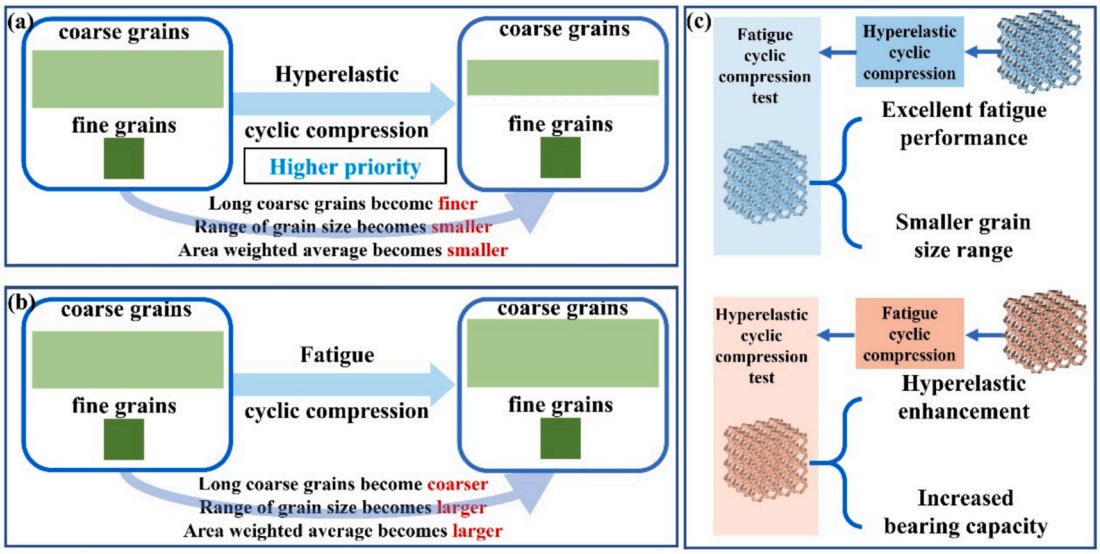

Fig. 9. Cyclic compression interaction mechanism: (a) hyperelastic cyclic compression; (b) fatigue cyclic compression; (c) the interaction between hyperelastic cyclic compression and fatigue cyclic compression.

its original subgrain structure provides support for further plasticity-induced refinement during cyclic loading. In contrast, the H_0F sample showed grain growth during fatigue loading due to the coarse initial grains and the lack of pre-formed subgrain network. This result is consistent with the observation results in other material systems, that is, at room temperature, cyclic loading can induce significant grain coarsening under the action of continuous stress field through mechanisms such as grain rotation and coalescence[51].

In the context of hyperelastic cyclic compression, moderate pre-hyperelastic cycles (H_2F) can introduce beneficial microstructural features[48] that delay crack initiation and early propagation. This is consistent with the findings of Mroziński et al.[52]. However, excessive pre-hyperelastic cycles (H_3F) will produce additional defects and reduce the beneficial effects of microstructure refinement[53]. Pelton et al.[54] also supported this behavior, pointing out that the effect of pre-strain may be beneficial or harmful, depending on the evolution of the microstructure. The fatigue life trend observed in this study: H_2F achieves the best balance between beneficial microstructure modification and avoiding excessive accumulation of defects; H_3F still benefits from pre-cycles, but to a lesser extent; H_1F is not enough to completely homogenize the microstructure; H_0F lacks any microstructure adjustment, resulting in the shortest fatigue life.

4. Conclusion

In this study, the interaction between hyperelastic cyclic compression and fatigue cyclic compression was designed, and the mechanical properties and fatigue properties of NiTi Gyroid lattice structure under cyclic compression were discussed. The main conclusions are as follows:

(1) The relative density of the sample reached more than 99 %. The NiTi Gyroid lattice structure fabricated by LPBF process has good forming quality.
(2) The fatigue cyclic compression pretreatment of 10^4 and 5×10^4 cycles is helpful to improve the hyperelasticity, while too many fatigue cycles will reduce the hyperelasticity. The bearing capacity of the sample is enhanced by 10^4 cycles of fatigue cyclic compression pretreatment, but shows a downward trend with the increase of the number of fatigue cycles.
(3) The appropriate cycles of hyperelastic cyclic compression pretreatment can enhance the fatigue resistance and deformation resistance of the NiTi lattice structure. The fatigue life of H_2F (the sample undergoes 8 cycles of hyperelastic cyclic compression and then fatigue cyclic compression) is 2.49 times that of H_0F (the sample is directly subjected to fatigue cyclic compression), and the fatigue life of H_3F (the sample undergoes 15 cycles of hyperelastic cyclic compression and then fatigue cyclic compression) is 1.73times that of H_0F.
(4) The fatigue performance of LPBF NiTi lattice structure can be further affected by reducing the grain size. There are coarse grains and fine grains in the microstructure of NiTi lattice prepared by LPBF. Hyperelastic cyclic compression improves the fatigue life of NiTi lattice structure by reducing the area weighted average of the grain size and reducing its size distribution range.

CRediT authorship contribution statement

Yunlong Ren: Writing – review & editing, Writing – original draft, Software, Methodology, Data curation. **Xiang Liu:** Methodology, Investigation, Conceptualization. **Lei Yang:** Visualization, Validation, Supervision, Resources, Project administration, Methodology, Funding acquisition. **Guanghui Yang:** Supervision, Formal analysis. **Liu He:** Visualization, Supervision, Formal analysis. **Lei Zhou:** Supervision. **Zhanpeng Pi:** Visualization. **Hejiang Xu:** Supervision. **Jinhua Xiao:** Validation, Funding acquisition. **Chunze Yan:** Visualization, Funding acquisition, Conceptualization. **Yusheng Shi:** Validation, Funding acquisition.

Declaration of Competing Interest

The authors declare that they have no known competing financial interests or personal relationships that could have appeared to influence the work reported in this paper.

Acknowledgements

The study was supported by the National Natural Science Foundation of China (No.52475398, 52235008, U2341270 and No.52305551) and Natural Science Foundation Project of Hubei Province (2024AFB767).

Data availability

The data that support the findings of this study are available from the corresponding author, [Lei Yang], upon reasonable request.

References

[1] Amadi A, Mohyaldinn M, Ridha S, et al. Advancing engineering frontiers with NiTi shape memory alloys: a multifaceted review of properties, fabrication, and application potentials. J Alloy Compd 2024;976:173227.
[2] Cloots M, Zumofen L, Spierings AB, et al. Approaches to minimize overhang angles of SLM parts. Rapid Prototyp J 2017;23(2):362–9.
[3] Zhang C, Qiao H, Yang L, et al. Vibration characteristics of additive manufactured IWP-type TPMS lattice structures. Compos Struct 2024;327:117642.
[4] Sun L, Chen K, Geng P, et al. Mechanical and shape memory properties of NiTi triply periodic minimal surface structures fabricated by laser powder bed fusion. J Manuf Process 2023;101:1091–100.
[5] Xiao JF, Cayron C, Van der Meer M, et al. EBSD study of variant reorientation, texture, and twin formation in a martensitic NiTi alloy deformed in compression. Acta Mater 2024;264:119553.
[6] Safdel A, Torbati-Sarraf H, Elbestawi MA. Laser powder bed fusion of differently designed NiTi stent structures having enhanced recoverability and superelasticity. J Alloy Compd 2023;954:170196.
[7] Elahinia MH, Hashemi M, Tabesh M, et al. Manufacturing and processing of NiTi implants: a review. Prog Mater Sci 2012;57(5):911–46.
[8] Yang L, Yan C, Han C, et al. Mechanical response of a triply periodic minimal surface cellular structures manufactured by selective laser melting. Int J Mech Sci 2018;148:149–57.
[9] Yang L, Yan C, Fan H, et al. Investigation on the orientation dependence of elastic response in Gyroid cellular structures. J Mech Behav Biomed Mater 2019;90:73–85.
[10] Yang L, Li Y, Chen Y, et al. Topologically optimized lattice structures with superior fatigue performance. Int J Fatigue 2022;165:107188.
[11] Zheng X, Guo X, Watanabe I. A mathematically defined 3D auxetic metamaterial with tunable mechanical and conduction properties. Mater Des 2021;198:109313.
[12] Hussain S, Alagha AN, Haidemenopoulos GN, et al. Microstructural and surface analysis of NiTi TPMS lattice sections fabricated by laser powder bed fusion. J Manuf Process 2023;102:375–86.
[13] Liu Q, Feng Y, Liu B, et al. Regulation of microstructure, phase transformation behavior, and enhanced high superelastic cycling stability in laser direct energy deposition NiTi shape memory alloys via aging treatment. Mater Sci Eng A 2024;915:147207.
[14] Sun X, Jiang F, Yuan D, et al. High damping capacity of AlSi10Mg-NiTi lattice structure interpenetrating phase composites prepared by additive manufacturing and pressureless infiltration. J Alloy Compd 2022;905:164075.
[15] Kara F, Ã–zbek N A Ã, Ã–zbek O Ã. Effect of Cryogenic Treatment on the Machinability of Impax Supreme Steel and Optimization of Machining Parameters [J]. ES Materials and Manufacturing, 2025, 27: 1457.
[16] Öztürk B, Kara F. Multi-Objective Optimization of Machinability and Energy Consumption of cast Iron depending on Cooling Rate. Machines 2025;13(2):84.
[17] Ren Y, Ran W, Li Y, et al. Enhancing the energy absorption capacity of Ti–6Al–4V lattice structure manufactured by additive manufacturing through β-annealing. J Mater Res Technol 2025;35:2369–76.
[18] Lee Y-L, Barkey ME, Kang H-T. Metal fatigue analysis handbook: practical problem-solving techniques for computer-aided engineering [M]. Amsterdam: Elsevier; 2011. p. 1–580.
[19] Kan Q, Zhang Y, Xu Y, et al. Tension-compression asymmetric functional degeneration of super-elastic NiTi shape memory alloy: Experimental observation and multiscale constitutive model. Int J Solids Struct 2023;280:112384.
[20] Safdel A, Zaker N, Botton GA, et al. The role of texture and restoration mechanisms in defining the tension-compression asymmetry behavior of aged NiTi alloys fabricated by laser powder bed fusion. Mater Sci Eng A 2023;864:144592.
[21] Wang Z, Feng C, Jiang D. Constitutive modeling of functional fatigue with tension–compression asymmetry for superelastic NiTi shape memory alloy. Int J Solids Struct 2024;305:113099.
[22] Yan A, Cai WS, Li HZ, et al. Stable superelasticity with large recoverable strain in NiTi alloy via additive manufacturing. Mater Sci Eng A 2024;911:146935.
[23] Zhang QQ, Sun WK, Gao MR, et al. Damage accumulation and its effect during thermal- and stress-induced cycling martensite transformation of laser powder bed fused (LPBF) NiTi alloy. Int J Fatigue 2024;186:108376.
[24] Bagheri A, Mahtabi MJ, Shamsaei N. Fatigue behavior and cyclic deformation of additive manufactured NiTi. J Mater Process Technol 2018;252:440–53.
[25] Kelly CN, Francovich J, Julmi S, et al. Fatigue behavior of As-built selective laser melted titanium scaffolds with sheet-based gyroid microarchitecture for bone tissue engineering. Acta Biomater 2019;94:610–26.
[26] Yang L, Yan C, Cao W, et al. Compression–compression fatigue behaviour of gyroid-type triply periodic minimal surface porous structures fabricated by selective laser melting. Acta Mater 2019;181:49–66.
[27] Luo J, Xu K, Li C, et al. The evolution of dynamic recrystallization and recrystallization texture during isothermal compression of NiTi shape memory alloy. Mater Sci Eng A 2021;820:141424.
[28] Lin D, Zhang C, Chen X, et al. TPMS_Scaffold_Generator: A Scaffold-Structure Generator based on Triply Periodic Minimal Surfaces. Additive Manufacturing Frontiers 2024;3(2):200123.
[29] Jin J, Wu S, Yang L, et al. Ni–Ti multicell interlacing Gyroid lattice structures with ultra-high hyperelastic response fabricated by laser powder bed fusion. Int J Mach Tool Manuf 2024;195:104099.
[30] Liu H, Lin D, Yang L, et al. Enhanced mechanical responses and fatigue behaviors of triply periodic minimal surface lattice metamaterials by twin-oriented lattice design. Int J Fatigue 2025;201:109172.
[31] Parsompech N, Suwanpreecha C, Noraphaiphipaksa N, et al. Supportless lattice structure of 316L stainless steel fabricated by material extrusion additive manufacturing: effect of relative density on physical, microstructural and mechanical behaviour. Mater Sci Eng A 2024;915:147270.
[32] Standard I. International Organization for Standardization. ISO 13314:2011. Mechanical Testing of Metals — Ductility Testing —Compression Test for Porous and Cellular Metals: [S]. Geneva: Switzerland, 2011:.
[33] Khorsandi F, Ayers PD, Truster TJ. Developing and evaluating a finite element model for predicting the two-posts rollover protective structure nonlinear behaviour using SAE J2194 static test. Biosyst Eng 2017;156:96–107.
[34] Yang L, Mertens R, Ferrucci M, et al. Continuous graded Gyroid cellular structures fabricated by selective laser melting: Design, manufacturing and mechanical properties. Mater Des 2019;162:394–404.
[35] Yang L, Ferrucci M, Mertens R, et al. An investigation into the effect of gradients on the manufacturing fidelity of triply periodic minimal surface structures with graded density fabricated by selective laser melting. J Mater Process Technol 2020;275:116367.
[36] Funch CV, Proust G. Laser-based additive manufacturing of refractory metals and their alloys: a review. Addit Manuf 2024;94:104464.
[37] Yang L, Li Y, Wu S, et al. Tailorable and predictable mechanical responses of additive manufactured TPMS lattices with graded structures. Mater Sci Eng A 2022;843.
[38] Xiang Z, Yang Q, Zhang T, et al. Tensile mechanical behavior of functionally graded NiTi alloy manufactured via laser powder bed fusion. Mater Sci Eng A 2024;914:147119.
[39] Mat Samudin I, Mohd Radzuan NA, Sulong AB, et al. Stress strain curve analysis of sheet based TPMS structures in quasi static compression test: a review. J Mater Res Technol 2025;36:5757–96.
[40] Khaniki HB, Ghayesh MH, Chin R, et al. Hyperelastic structures: a review on the mechanics and biomechanics. Int J Non Linear Mech 2023;148:104275.
[41] Sedmák P, Šittner P, Pilch J, et al. Instability of cyclic superelastic deformation of NiTi investigated by synchrotron X-ray diffraction. Acta Mater 2015;94:257–70.
[42] Chen J, Liu F, Fang G, et al. Intermittent healing for alleviating the functional fatigue and restoration of the elastocaloric effect in superelastic NiTi shape memory alloy. Journal of Materials Science & Technology 2025;227:289–303.
[43] Prevéy PS, Cammett JT. The influence of surface enhancement by low plasticity burnishing on the corrosion fatigue performance of AA7075-T6. Int J Fatigue 2004;26(9):975–82.
[44] Ren Y, Li Y, Yang L, et al. Compressive properties and fatigue performance of NiTi lattice structures optimized by TPMS. MSAM 2024;3(2):3380.
[45] Zhang Y, Yang L, Yu L, et al. Ni-Ti-Zr ternary alloy with high transition temperature fabricated by laser powder bed fusion. J Alloy Compd 2023;938:168529.
[46] Toghani-Taheri F, Khodabakhshi F, Malekan M, et al. Cyclic pseudoelastic behavior of friction stir processed NiTi shape memory alloy: Microstructure and W-alloying. Mater Sci Eng A 2025;927:148000.
[47] Guo C, Shao S, Wang S, et al. Microstructural evolution and mechanical properties of additively manufactured NiTi shape memory alloys: the role of scanning speed variation. J Alloy Compd 2025;1025:180344.
[48] Song M, Qiu Y, Xu B, et al. Fatigue failure and grain refinement strengthening mechanism of aluminum alloy weld. Int J Fatigue 2025;197:108950.
[49] Fintová S, Kunz L, Chlup Z, et al. Grain refinement effect on fatigue life of two grades of commercially pure titanium. Int J Fatigue 2023;176:107883.
[50] Christison A, Paranjape H, Daly S. Plasticity Bridges Microscale Martensitic Shear Bands in Superelastic Nitinol. Exp Mech 2025:1–18.
[51] Goswami R, Feng C, Qadri S, et al. Fatigue-assisted grain growth in Al alloys. Sci Rep 2017;7(1):10179.
[52] Mroziński S, Piotrowski M, Egner W, et al. Influence of Pre-Strain on the Course of Energy Dissipation and Durability in Low-Cycle Fatigue. Materials 2025;18(4):893.
[53] Polák J. Role of persistent slip bands and persistent slip markings in fatigue crack initiation in polycrystals. Crystals 2023;13(2):220.
[54] Pelton A, Berg B, Saffari P, et al. Pre-strain and mean strain effects on the fatigue behavior of superelastic nitinol medical devices. Shape Mem Superelasticity 2022;8(2):64–84.